Vol. 89 No. 1 pp. 90–104 ACTA GEOLOGICA SINICA (English Edition) Feb. 2015

Lithospheric Electrical Structure across the Eastern Segment of the Altyn Tagh Fault on the Northern Margin of the Tibetan Plateau

ZHANG Letian[1, 2], YE Gaofeng[1, 2, *], JIN Sheng[1, 2], WEI Wenbo[1, 2, 3], Martyn UNSWORTH[4], Alan G. JONES[5], JING Jianen[1, 2], DONG Hao[1, 2], XIE Chengliang[1, 2], Florian LE PAPE[5] and Jan VOZAR[5]

1 *School of Geophysics and Information Technology, China University of Geosciences, Beijing* 100083, *China*
2 *Key Laboratory of Geo-detection of Ministry of Education, Beijing* 100083, *China*
3 *State Key Laboratory of Geological Processes and Mineral Resources, Beijing* 100083, *China*
4 *Department of Physics, University of Alberta, Edmonton, Alberta, Canada*
5 *Dublin Institute for Advanced Studies, Dublin, Ireland*

Abstract: Project INDEPTH (InterNational DEep Profiling of Tibet and the Himalaya) is an interdisciplinary program designed to develop a better understanding of deep structures and mechanics of the Tibetan Plateau. As a component of magnetotelluric (MT) work in the 4th phase of the project, MT data were collected along a profile that crosses the eastern segment of the Altyn Tagh fault on the northern margin of the plateau. Time series data processing used robust algorithms to give high quality responses. Dimensionality analysis showed that 2D approach is only valid for the northern section of the profile. Consequently, 2D inversions were only conducted for the northern section, and 3D inversions were conducted on MT data from the whole profile. From the 2D inversion model, the eastern segment of the Altyn Tagh fault only appears as a crustal structure, which suggests accommodation of strike slip motion along the Altyn Tagh fault by thrusting within the Qilian block. A large-scale off-profile conductor within the mid-lower crust of the Qilian block was revealed from the 3D inversion model, which is probably correlated with the North Qaidam thrust belt. Furthermore, the unconnected conductors from the 3D inversion model indicate that deformations in the study area are generally localized.

Key words: magnetotellurics, northern margin of the Tibetan Plateau, eastern segment of the Altyn Tagh fault, lithospheric electrical structure

1 Introduction

The total area of the Tibetan Plateau is approximately 2.6 million square kilometers, and the average elevation is approximately 4000 m. Because of its unique geological features, the Tibetan Plateau has become the focus of studies on global change, geodynamics, and many other research subjects, and it is an ideal place to investigate the material and energy exchanges that occur deep within the Earth, as well as the interactions of various spheres (Burchfiel, 2013; Xu et al., 2013). It is of great scientific value to study the telluric structure of the Tibetan Plateau and to reveal its uplift process and the mechanism of its interaction with adjacent plates. All of these questions are related to the process of mass transportation deep within the Tibetan Plateau. The magnetotelluric (MT) method uses the natural electromagnetic field, which possesses rich spectral components, as its source field. This approach can detect the electrical structures (resistivity or conductivity) of underground matter on the lithospheric scale. The natural MT field readily penetrates resistive regions and is very sensitive to the presence of conductive bodies. Therefore, the MT field can effectively reflect the distribution of deep fluid and high temperature regions and plays an important role in the constraint of rheological structures inside the lithosphere. By applying the MT method to probe the electrical structure of the crust and mantle deep within the plateau, we can provide important information of electrical properties toward solving the aforementioned problems; as a result, we can further understand the tectonic features and processes of mass

* Corresponding author. E-mail: ygf1999@cugb.edu.cn

transportation that occur deep within the plateau, which might help to solve the significant scientific questions mentioned above.

Within the last twenty years, scientists have carried out numerous studies of MT measurements in the Tibetan Plateau area. The InterNational Deep Profiling of Tibet and the Himalaya (INDEPTH) project, which began in 1992, examined the characteristics of the crust and mantle structures inside the Tibetan Plateau using near-vertical deep reflection seismic, MT sounding, and other geophysical methods. The 4-stage study has accomplished geophysical measurements across the Tibetan Plateau, from south to north, and has obtained significant results that are recognized by the international scientific community (Nelson et al., 1996; Wei et al., 2001; Tilmann et al., 2003; Unsworth et al., 2005; Karplus et al., 2011; Le Pape et al., 2012; Mechie et al., 2012; Karplus et al., 2013). The MT research carried out by the INDEPTH program began in 1995, obtaining the data and distribution model of crust-mantle electrical resistivity from 12 MT profiles through studies performed over a decade. These studies, together with a series of MT sounding profiles later obtained independently by research groups in China (Tan et al., 2004; Wei et al., 2006a; 2006b; 2009; Jin et al., 2006; 2007; 2009; Ye et al., 2007), further demonstrated that the plateau has a very unique crust-mantle electrical structure, which has attracted significant attention. According to the research results presented over the last ten years, intra-crust high-conductivity bodies are prevalent within the Tibetan Plateau. Although intra-crust high-conductivity bodies in different regions are similar in size, depth and conductivity, the distinct local differences among such bodies are closely related to the regional tectonic patterns and distribution of fault zones. A preliminary inference suggested that the presence of these intra-crust high-conductivity bodies is related to the partial melting body and thermal fluid present deep within the plateau. The collision between the Indian Plate and Asian Plate has caused Tibetan Plateau uplift since the Cenozoic era. The subduction of the Indian Plate formed the “double crust” in the Tibetan Plateau and, consequently, the very thick lithosphere. Therefore, it is highly likely that the rock deep within the Tibetan Plateau has partially molten to form materials that are rheologically flowable. The Phase IV study of the MT sounding of INDEPTH was mainly focused on the Altyn Tagh fault (ATF) on the northern margin of the Tibetan Plateau. In this paper, we mainly used the broadband and long-period MT data obtained from the eastern segment of the ATF during INDEPTH-IV to derive the lithospheric electrical structures in this area and to further analyze the deep tectonic characteristics based on the electrical structure; these results provided strong constraints and evidence for the study of deep rheological structures and the deformation mechanism in this area from the aspect of electrical properties.

2 Overview of the Study Region

The sinistral strike-slip ATF located on the northern margin of the Tibetan Plateau presents a distinct boundary in terms of surface topography. To the south of the ATF is the Tibetan Plateau, with an average elevation of approximately 4000 m. To its north is the Tarim Basin, with an average elevation of only approximately 1000 m. This large elevation difference implies complex deep structural conditions. It is commonly accepted that the ATF begins in the west at the Pamir Mountains and ends in the east near the Qilian Mountains, with a full length of ~1500 km. Generally, the ATF is divided into three sections, identified as the west, middle, and east, using the longitudinal coordinates 84°E and 94°E as the boundaries. Strong coupling has occurred between the eastern ATF (east of 94° E) and the Qilian tectonic domain, as evidenced by a series of NW-SE trending thrust faults distributed along the northeastern margin of the Qaidam Basin (Washburn et al., 2003) (see Fig. 1). It is generally believed that, in the eastern ATF, the sinistral strike-slip movements occurring along the ATF were gradually converted into a series of thrusting movements in the Qilian tectonic domain. In the eastern ATF, where the study presented in this paper was conducted, the sinistral shearing along the ATF has resulted in the formation of a regional Precambrian metamorphic zone and has separated the sedimentary layer of the Qaidam Basin from the Tarim block with Precambrian basement. Meanwhile, sporadic Jurassic coal-bearing sedimentary layers also appear in the study area (Chen et al., 2003).

As the active strike-slip fault system that constrains the northern margin of the Tibetan Plateau, the ATF plays an important role in the absorption of the collision between the Indian Plate and the Eurasian Plate. Zhang et al. (2004) constructed the velocity field of the current tectonic deformation in the Tibetan Plateau using GPS data. The velocity distribution indicates that the relative movement between the Indian Plate and the Eurasian Plate is mainly adjusted and absorbed by crustal shortening and internal strike-slip shearing in the peripheral area of the Tibetan Plateau. In particular, the Himalaya Mountains absorbed 44%–53% of the total shortening of the Tibetan Plateau, while the Qaidam Basin, Qilian Mountains, and Altyn Mountains in the north absorbed 15%–17%, and the interior of the plateau absorbed the remaining 32%–41%. Current studies generally believe that the sinistral strike-

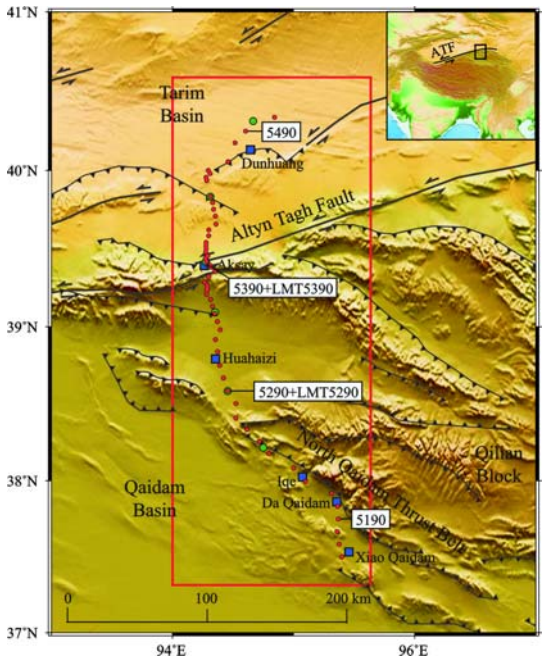

Fig. 1. Topography map showing MT stations layout and tectonic structures in the survey area.
Red dots are broadband stations, green dots are long period stations, tectonic structures are after Styron et al. (2010). Red rectangle shows the region of 3D inversion.

slip displacement of the ATF that has occurred since the Oligocene is approximately 475 km (Peltzer and Tapponnier, 1988; Ritts and Biffi, 2000; Cowgill et al., 2003). There is significant controversy regarding the measurement results of the slip rate along the ATF. The results from different measurement methods range from 10–20 mm/yr, and the difference is on the order of several fold (Bendick et al., 2000; Shen et al., 2001; Wallace et al., 2004; Mériaux et al., 2004; 2005; Zhang et al., 2007; Elliott et al., 2008; Cowgill et al., 2009; Gold et al., 2011). However, a significant point is that the slip rate exhibits a gradual decreasing trend toward the east. Meyer et al. (1996) summarized that the slip rate along the ATF to the east of 96°E is only 4±2 mm/yr. It is believed that this trend is caused by the gradual absorption of the sinistral strike-slip movement along the ATF by the thrust fault system at the periphery of the Qaidam Basin (Peltzer et al., 1989; Chen et al., 1999).

Previous studies on the eastern ATF have mainly applied the MT method. Bedrosian et al. (2001) probed the main fault structure of the eastern section as a subvertical interface of electrical resistivity extending to at least 8 km deep based on four MT sounding profiles. However, because the MT data were mainly collected for oil exploration, they are mainly specific to the interior of the Tarim Basin. Only the southern end of the profiles cross the ATF, and the collection period was relatively short. The corresponding exploration depth is not deep enough; thus, the tectonic problems that can be solved are very limited. In recent years, Xiao et al. (2011) deployed three MT profiles in the area of the eastern ATF and the southern part of the Qilian Mountains; the authors derived the lithospheric electrical structure model in the study area through 2D and 3D inversion. The results indicate that the lithospheric electrical structure of the eastern ATF varies horizontally and that the positive flower structure generated by the shearing action gradually weakens toward the east. The overall Tarim block exhibits significant resistive, which reflects the underthrust trend of the cold rigid Tarim block beneath the main ATF. Additionally, large-scale conductors were found at the depth range of Moho in the area to the south of the ATF, which might correspond to the weak layer inside the Tibetan Plateau. However, because of the limited southward extension of the profile, it cannot reflect the extension of this conductive layer toward the interior Tibetan Plateau. In summary, controversy still exists regarding many issues developed in previous studies, such as the geometry of the fault system at depth, cutting depth of the main fault, the existence of a widespread weak layer beneath the Qaidam Basin, as well as the slip rate along the ATF. Although MT sounding investigations have been carried out in the eastern ATF, all of the existing profiles are insufficient relative to the southward extension. From the perspective of MT sounding, the obtained model of lithospheric electrical structure through this study can be used to constrain and further solve the aforementioned problems.

3 MT Data Collection and Processing

The distribution of surveyed sites is shown in Fig. 1. The MT sounding profile was mainly deployed along the northeastern margin of the Qaidam Basin to detect the crust-mantle electrical structure of the passing area. The profile section begins in the north near Dunhuang, passes through the main ATF in the Aksay section and extends southward through Hua Haizi, Iqe, and Da Qaidam, ending near Xiao Qaidam on the northeastern margin of the Qaidam Basin. The data collection in the field was accomplished in the summers of 2009 and 2010, respectively, and they include a total of 55 broadband stations and 6 long-period stations. For broadband data collection, we used the MTU-5 instruments manufactured by the Phoenix Company of Canada, which has an average dot pitch of 5 km and an average acquisition time of 20 hours, and for which the processed period range of useful signal is 0.003–2000 s. The long-period data were collected using the LEMI-417 instruments developed by the LVIV Center of Ukrainian Institute for Space

Research, which has an average inter-site distance of 40 km and an average collection interval of 20 days, and for which the processed frequency range of useful signal is approximately 100–10000 s. Based on the rational combination of these two types of sounding stations, we can derive the electrical data set covering the entire lithospheric scale. Data collection in the field was based on a cross-shaped deployment for tensor acquisition, and a total of five components, including horizontal electric fields and horizontal and vertical magnetic fields (Ex, Ey, Hx, Hy, and Hz), were collected. The original time series was converted from the time domain to the frequency domain by Fast Fourier Transform and then further converted to high-quality impedance tensor data through a series of standardized processes, including remote reference (Gamble et al., 1979), Robust estimate (Egbert et al., 1997) and power spectrum selection.

Figure 2 shows the sounding curves at six typical survey locations, where 5190, 5290, 5390 and 5490 are broadband stations, and LMT5290, LMT5390 are long-period stations. All survey locations are indicated in Fig. 1. It can be seen that the sounding data are generally of relatively high quality. It also should be noted that the broadband station and long-period station do not completely overlap (although some of the broadband stations and long-period stations are very close in location) because they were not deployed in the same year. Therefore, in the following data analysis and inversion process, the long-period stations are treated as independent stations and are not combined with the broadband stations data. Moreover, the sounding curve in Fig. 2 is unedited and not rotated; some of the flying points in the curve were eliminated in the subsequent data editing process.

4 MT Data Analysis

4.1 Phase tensor analysis

After obtaining the impedance tensor data, the dimensionality of the acquired data must be analyzed to determine further the appropriate method of data processing and inversion (1D/2D/3D). In this paper, we used the phase tensor tool (Caldwell et al., 2004; Moorkamp, 2007) to analyze the dimensionality of the profile data. The phase tensor in the dimensional analysis of the MT data is less susceptible to the impact of 3D distortion effects; its diagram can be expressed as an

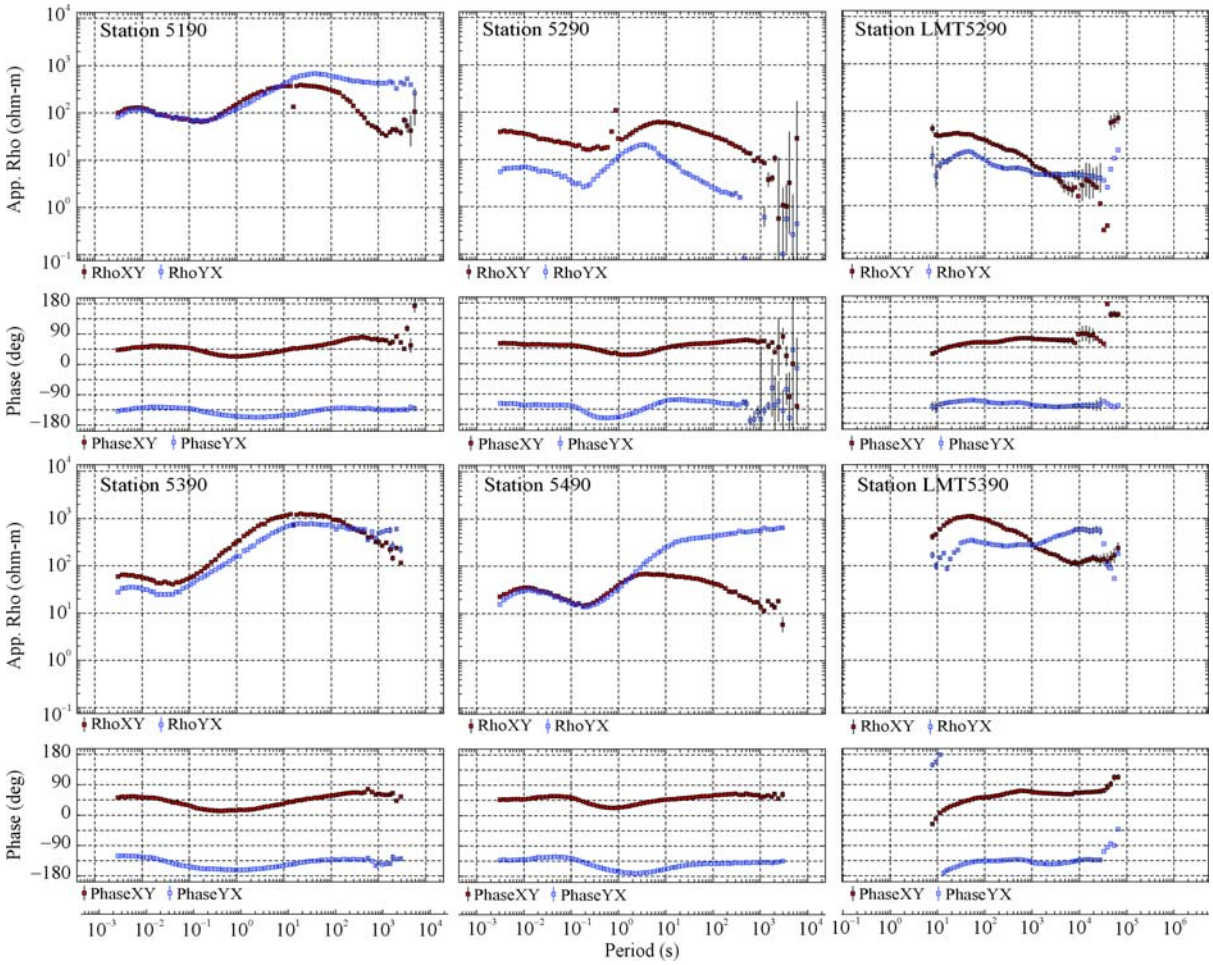

Fig. 2. Apparent resistivity and phase curves of the typical stations (see Fig. 1 for the station locations).

ellipse in which the directions of the long and short axes of the ellipse correspond to the directions of the two main electrical axes, which are perpendicular to each other. Generally, as the long axis and short axis of the ellipse approach each other in length, the one-dimensionality increases, with the ellipse degenerating to a circle under an ideal one-dimensional scenario. Additionally, each ellipse of the phase tensor corresponds to a 2D skew angle β, and larger values of β indicate stronger three-dimensionality of the MT data. Figure 3 shows the distribution of phase tensors for four periods, 0.1 s, 10 s, 100 s, and 1000 s. As shown in the figure, at the shallow mid-high frequency bands (0.1 s and 10 s, as shown in Fig. 3a-b), the 2D skew angle β at the majority of the stations along the profile section is smaller than 5° (the blue color), which indicates that the profile data exhibit good one-dimensionality. In particular, some stations inside the Tarim Basin to the north and the Qaidam Basin to the south of the profile section (as shown in Fig. 3a) possessed dimensionality values that were very close to the 1D situation (the ellipse

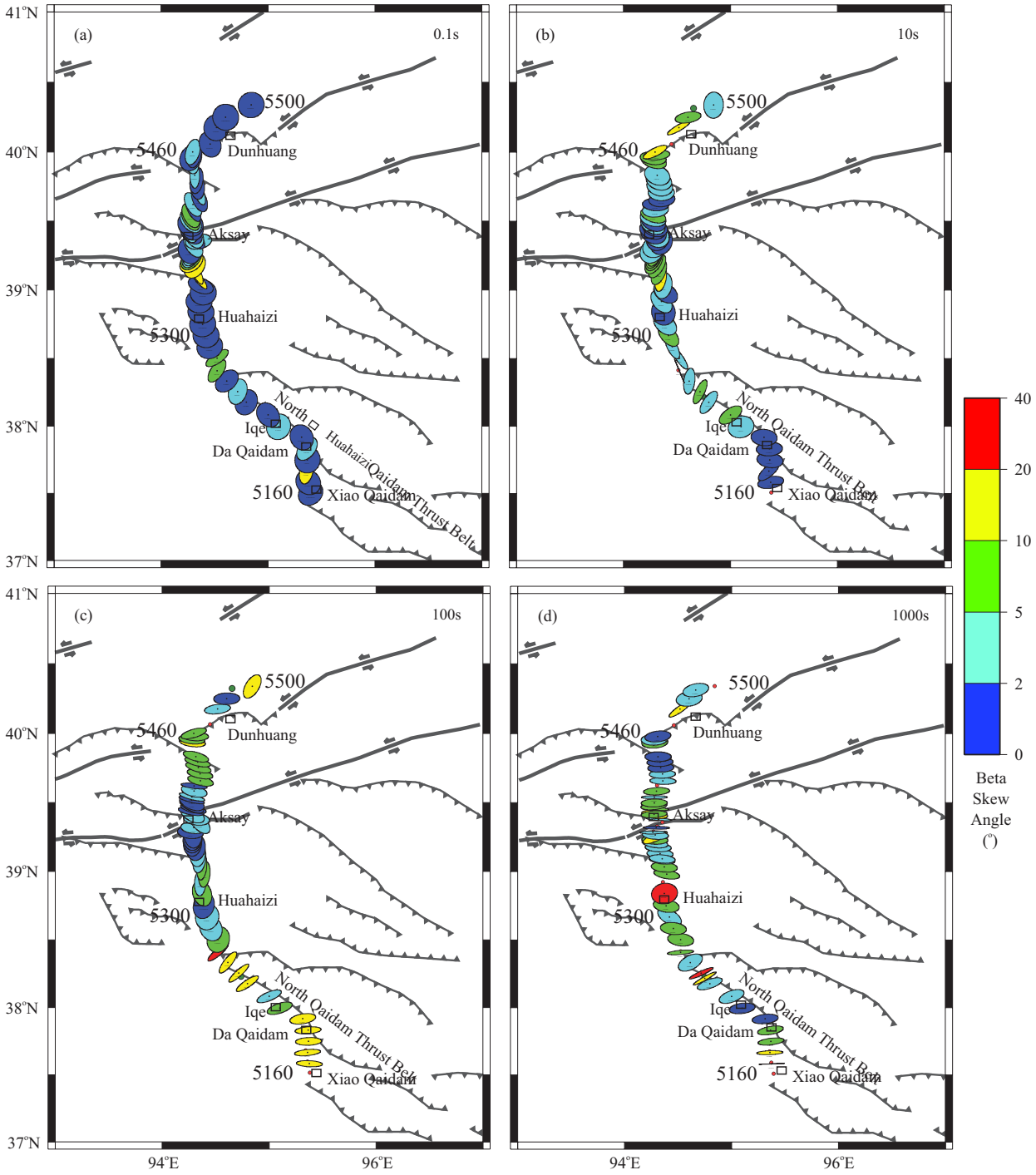

Fig. 3. Phase tensor maps for 4 different periods.

nearly degenerated to a circle), which indicates that the shallow sedimentary layer in these areas has significant 1D features. In the low-frequency band (100 s and 1000 s, as shown in Fig. 3c-d), some stations from the profile exhibited a certain degree of three-dimensionality (β>10°, as shown by the red or yellow color), which indicates that the tectonic structure in these areas is relatively complicated and exhibits 3D effect. The southern section of the profile located between stations 5160 and 5300 exhibits strong regional three-dimensionality near 100 s (as shown in Fig. 3c), which most likely indicates the presence of a regional 3D structure. This regional 3D structure is likely associated with the thrust belt along the northern margin of the Qaidam Basin. The high-pressure to ultra-high-pressure metamorphic zone distributed along this thrust belt (Zhang et al., 2007) indicates that there may be some regional structures deep in this area that lie basically parallel to the profile, which could be the main origin of the three-dimensionality of the MT data. Therefore, the traditional 2D processing and inversion method is no longer applicable to these MT data in the southern section of the profile. In comparison with the southern section, the northern section of the eastern profile (to the north of station 5300) maintains good overall two-dimensionality and is suitable for 2D inversion. Based on the result of this analysis, we implemented 2D inversion for the northern section (5300–5460) of the profile and implemented 3D inversion for the overall data set.

4.2 Impedance tensor decomposition

Before performing 2D inversion on the data set, it is necessary to determine the regional strike direction in the area passed by the profile. Then, the MT data can be decomposed into two independent polarized modes, namely, the transverse electric mode (TE) and the transverse magnetic mode ™. In this paper, we used the multi-site, multi-frequency impedance tensor decomposition technique developed by McNeice and Jones (2001) based on Groom-Bailey's (1989) decomposition method, and we obtained the distribution of electrical principal axis for all stations within the study area. The results of our analysis indicate that the distribution of electrical principal axis for the entire profile is complicated, and it was very difficult to derive a unified result; this difficulty may be related to the complicated geological tectonic conditions in this area, which are controlled by both the ATF in the north and the Qilian tectonic domain in the south. As shown by the rose diagram in the upper part of Fig. 4, the high-frequency data (0.01–0.1 s) reflect the shallow nature of the structure and indicate that the strike direction is approximately parallel to the surface trending of the ATF, which is

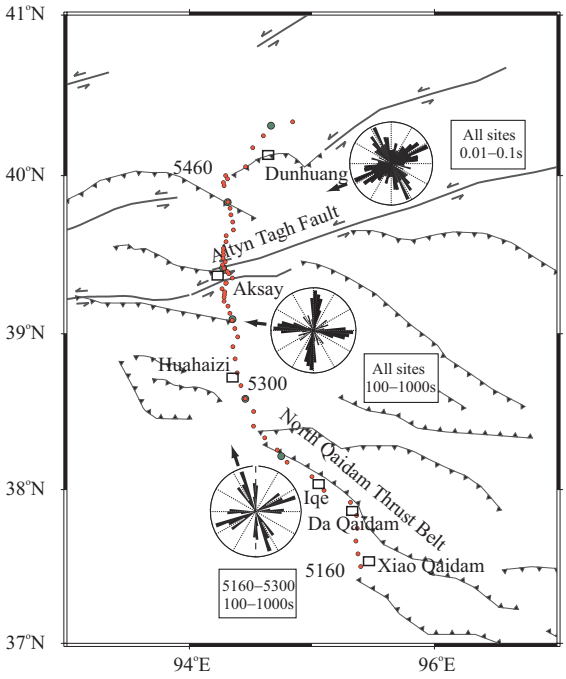

Fig. 4. Strike analysis results at different period bands and a comparison with regional tectonic structures.

approximately 60°NE. As the period increases, the low-frequency data (100–1000 s) reflecting the deep structure indicate that the strike direction gradually exhibits a trend that is approximately parallel to the thrust faults to the south of the ATF (as shown by the rose diagram at the center of Fig. 4). This indicates that the regional strike direction rotates with changing depth. Previous MT research carried out in the same area observed a similar feature (Bedrosian et al., 2001). Additionally, another noteworthy phenomenon is that the northern and southern sections of the profile most likely have different strike directions in the long-period range (100–1000 s). The distribution of electrical principal axis between stations 5160 and 5300 in the southern section of the profile, most likely reflects the tectonic trending direction of the thrust belt on the northern margin of the Qaidam Basin (as shown by the lower rose diagram in Fig. 4), which is essentially perpendicular to the surface trend of the ATF. What should be noted is that the strike direction determined by the distribution of electrical principal axis has an uncertainty of 90°. Hence, it is necessary to apply other information to determine which direction is the exact strike direction.

4.3 Induction vector analysis

The induction vector is an essential parameter for the analysis of MT data, and it is defined as the complex ratio between the vertical magnetic field and the horizontal magnetic field. This parameter is most sensitive to lateral variation in the conductivity of subsurface substance.

Under Parkinson's (1959) convention, the induction vector points to the region in which the current converges, namely, the location of high conductivity. Induction vector analysis can be used to determine the location of conductive bodies near the measurement site and to determine the two-dimensionality of the data. Under the ideal 2D condition, the distribution of conductive bodies should extend infinitely along the strike direction; thus, the direction in which the induction vector points should be perpendicular to the 2D strike direction. Figure 5 shows the distribution of induction vectors in two frequency bands of 10–100 s and 100–1000 s. According to this figure, the induction vector distribution in the southern section of the profile indicates the presence of a regional 3D structure in this area, thus the induction vector arrows point in the direction of the thrust belt in the Qilian tectonic domain. This feature also indicates that the regional strike direction of the southern section of the profile should be roughly parallel with the trending of the profile (or perpendicular to the direction of the induction vectors), as well as similar to the surface trending of the North Qaidam thrust belt. In contrast, the direction in which the induction vectors point in the northern section of the profile is approximately perpendicular to the surface trend of the ATF, demonstrating good two-dimensionality. Based on this information, it was eventually determined that the regional strike direction in the northern section of the profile is NE 60°, which is mostly consistent with the surface trending of the ATF. Additionally, the impedance tensor data were decomposed and inverted according to this direction. Based on the analysis above, the controlling depth of the ATF is shallow in the study area, whereas a series of NW-SE trending thrust faults in the Qilian tectonic domain most likely control the deep structure of the southern section of the profile. Generally speaking, the southern section of the profile has strong 3D features, and thus the traditional 2D analysis and inversion approach are no longer applicable to this region.

5 MT Data Inversion

5.1 Two-dimensional (2D) inversion

Based on the analysis above, we conducted a 2D nonlinear conjugate gradient (NLCG) (Rodi and Mackie, 2001) inversion study for the data of the northern section of the profile (5300–5460). We conducted numerous inversions for the data of different modes (TE, TM, tipper, TE+TM, TM+tipper, and TE+TM+tipper) under different parameter settings. The inversion process indicated that the RMS misfit is generally large (generally >3) for all of the 2D inversion results involving TE mode data. These inversion results only reflect some conductive features of the shallow uppermost crust, and the electrical structure of the rest of the profile manifested almost entirely as high-resistivity, which is apparently unreasonable. A similar problem arose for the other inversion results (such as TE+TM and TE+TM+ tipper) involving TE mode data. This unreasonable inversion result most likely indicates

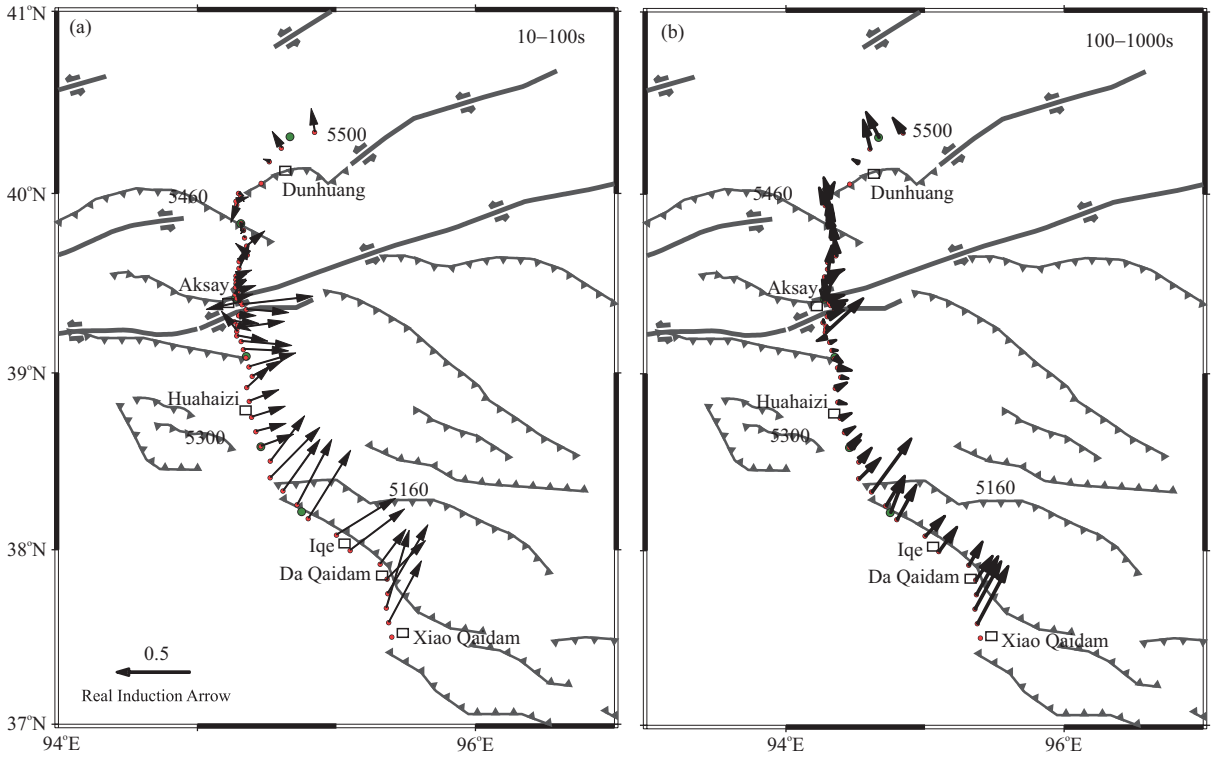

Fig. 5. Induction vector maps at 10–100 s (a) and 100–1000 s (b).

that the TE mode data were affected by the 3D distortion effect. Through forward studies, Cai and Chen (2010) found that for the 2D inversion of MT data generated from a 3D model, the degree of 2D approximation of the model required by the TE mode data is significantly higher than that by the TM mode data; when the influence of the 3D structure is obvious, it is more reasonable to use TM mode data for the 2D inversion than other modes, delivering fewer false anomalies in the inversion result. Therefore, the TM mode data should be given priority for the 2D inversion. Generally, the TM mode data better reflect the 3D structures that are approximately parallel to the 2D regional strike direction (Ledo, 2005) and are less susceptible to the distortion effect caused by off-profile 3D conductors (Berdichevsky, 1999). The previous MT studies carried out in the same area also mostly used the inversion result of the TM mode data as the final model and for interpretation (Bedrosian et al., 2001; Xiao et al., 2011). Therefore, the regional 3D distortion effect in this area seems to be a common feature; as a result, the TE mode data are strongly affected by the significant distortion effect.

In comparison with the TE mode data, the independent inversion results of the TM mode data and tipper data are more reliable. Both can be used to derive smooth model with a good fitting (the RMS misfit is <2), and the reflected main electrical characteristics are also consistent. Therefore, in this paper, we selected the reversion result of TM+tipper with a low misfit as the final 2D inversion model, as shown in Fig. 6a. The parameter settings used in the inversion are as follows: the error floor for TM apparent resistivity is 10%, the error floor for TM phase is 5%, the absolute error for tipper data is 0.05, and the regularization factor is τ = 3. The inversion process applied the MT data for a total of six decades of period from 0.01 to 10000 s. The initial model is a 100-Ωm uniform half space. After 200 iterations, the final RMS misfit is 1.729. Additionally, Figures 6b-I show the pseudo-sections of the measured TM apparent resistivity, phases, real and imaginary part of the tipper data, and their corresponding response data. The comparison shows that the

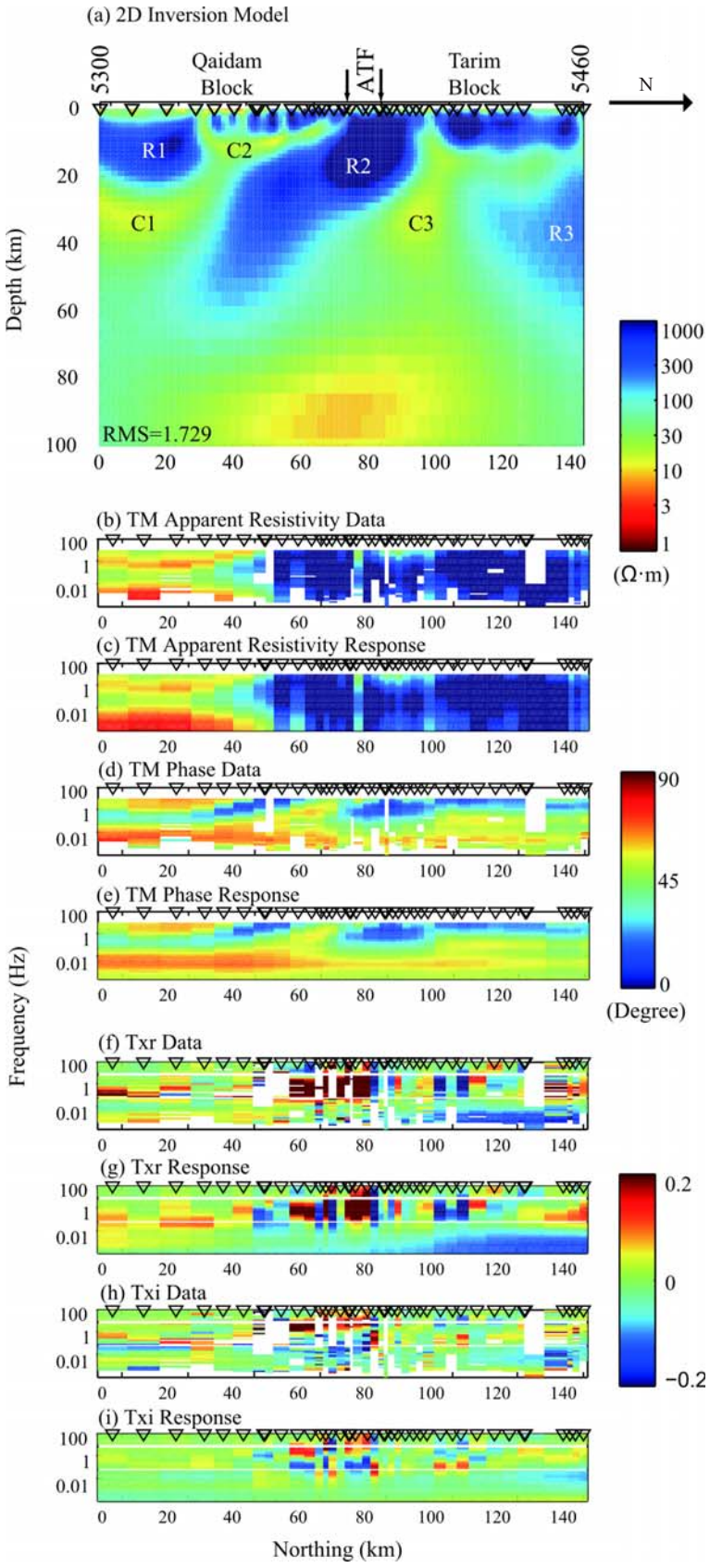

Fig. 6. 2D inversion model for the northern section of the profile (a) and pseudosections of observed and modeled data (b-i).
C – Conductors; R – Resistors; ATF – Altyn Tagh Fault.

measured data are very close to the response data generated from the inversion model, which indicates that an ideal fitting has been obtained and that the inversion model is reliable.

5.2 Three-dimensional (3D) inversion

In recent years, following the rapid development of computational science, the 3D inversion of MT data has overcome the previous bottleneck that existed due to the constraints of computing conditions and can now be increasingly used (Siripunvaraporn, 2011; Miensopust et al., 2013). Normal 3D MT inversion mainly uses the 3D data set acquired in the form of a grid network. However, 3D inversion is also applicable for the MT data set acquired in the form of a 2D profile. Three-dimensional inversion of MT sounding data for a 2D profile has the following advantages: (1) it is not necessary to determine the regional strike direction in advance of conducting 3D inversions; and (2) a 3D inversion with full impedance tensor data can qualitatively reflect the distribution of off-profile electrical anomalies in addition to the underground electrical structure beneath the profile region (Siripunvaraporn et al., 2005b). The aforementioned properties of 3D inversion are not present in traditional 2D inversion. Furthermore, in this case, 3D inversion is essential to resolve the lithospheric electrical structures due to the complex dimensionality and directionality in the study area. Therefore, in this study, we also implemented 3D inversion for the profile data. However, because of the limitations associated with computational conditions, the 3D inversion model cannot be discretized as finely as the 2D model. To save memory and improve the computational efficiency, the number of station data and frequency points for each station were both reduced for 3D inversions.

3D inversion was performed using the WSINV3DMT code developed by Siripunvaraporn et al. (2005a) based on the REBOCC algorithm. The number of meshed grids is 56×56×35 (south-north × east-west × vertical). The initial model is a 100-Ωm uniform half-space. We selected 49 broadband stations with high quality data from the profile for the inversion, including broadband stations in the southern section of the profile that were not used in the 2D inversion. We further reduced the frequency points in 1–1000 s to 9 for the selected stations (approximately 3 frequency points on each decade of period). To derive as much electrical structure information as possible through the 3D inversion regarding the off-profile structures, we employed the full impedance tensor data during inversion (including the real and imaginary parts of Zxx, Zxy, Zyx, and Zyy, giving a total of 8 components). The parameters used in the 3D inversion are as follows: the parameter of the length scale that controls the characteristic of model covariance was $\tau=5$, $\delta x=\delta y=\delta z=0.1$, and the initial Lagrange multiplier was $\lambda=1$ with step=0.5. After 10 iterations, the final RMS misfit of 3D inversion is 2.94. Selected horizontal and vertical slices from the final 3D inversion model are shown in Fig. 7.

5.3 Inversion results

The 2D inversion model of the profile is shown in Fig. 6a. The electrical structure is approximately divided into three resistors (R1, R2, and R3) and three conductors (C1, C2, and C3). The shallow part of the Qaidam block in the 2D model is mainly constituted by the northern conductor C2 and the southern resistor R1. According to the distribution pattern of C2, this body may connect with the conductor C1 located under R1 to form a south-dipping conductive layer. The electrical structure under the main ATF is mainly constituted of the south-dipping resistor R2. To the north of the main ATF, the deep part of the Tarim block is mainly constituted by a conductor C3 located in the south and the resistor R3 located in the north.

3D inversion of the 2D profile can qualitatively reflect some of the off-profile electrical structures, especially the high-conductivity bodies (Siripunvaraporn et al., 2005a). From the horizontal slices of the 3D inversion model (Fig. 7a), two main off-profile conductors were marked as C4 and C5. These two conductors only manifest in the 3D inversion model. C4 is located within the range of the mid-upper crust inside the Qaidam block to the north of thrust T1, and C5 is located within the range of the mid-lower crust inside the Qilian block to the east of the North Qaidam thrust belt. As analyzed in section 4.3 of this paper, the induction vectors at stations in the southern section of the profile generally point toward the off-profile thrust belts inside the Qilian tectonic domain (as shown in Fig. 5); this abnormal induction vector phenomenon is explained well by the existence of large-scale conductor C5. Figures 7b and 7c give the vertical slices through conductors C4 and C5. It can be seen that the distributions of these two conductors are associated with thrust T1 and the North Qaidam thrust belt, respectively. The northern section of the vertical slice showed in Fig. 7b roughly overlaps with the northern section of the profile from the 2D inversion. A comparison between the 2D model and the 3D model given in Fig. 8 shows that their electrical structure distributions are consistent, except for the low resolution of the 3D model. This also further demonstrates the reliability of the 2D inversion model for the northern section of the profile. Because the 3D inversion model is coarser and the fitting error is higher compared with the 2D model, the main model interpreted for the research in this paper is based on the results of 2D inversion. The 3D

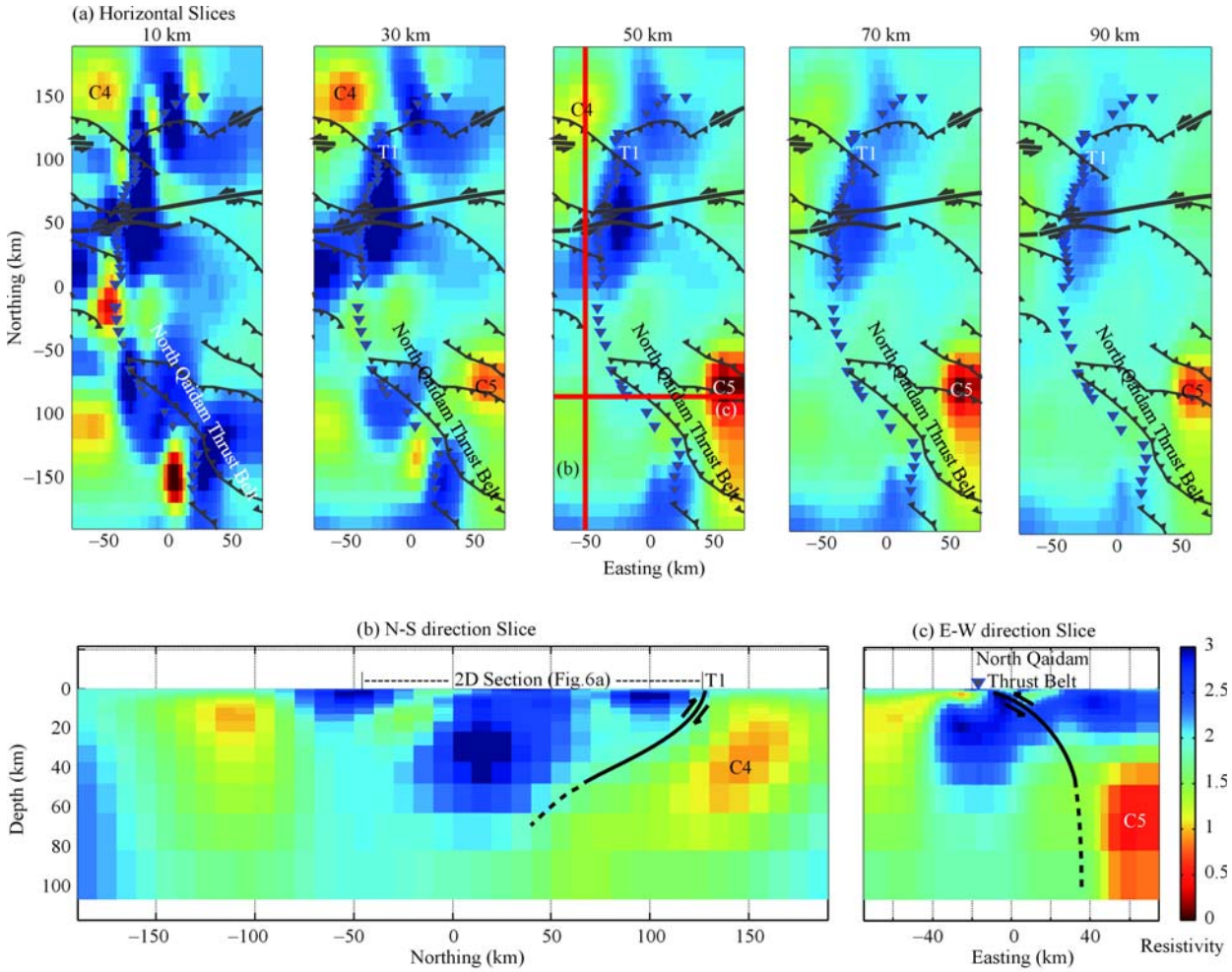

Fig. 7. Horizontal slices (a); north-south direction slice (b) and east-west direction slice (c) from the 3D inversion model.
T1 is thrust structure, C4 and C5 are conductors.

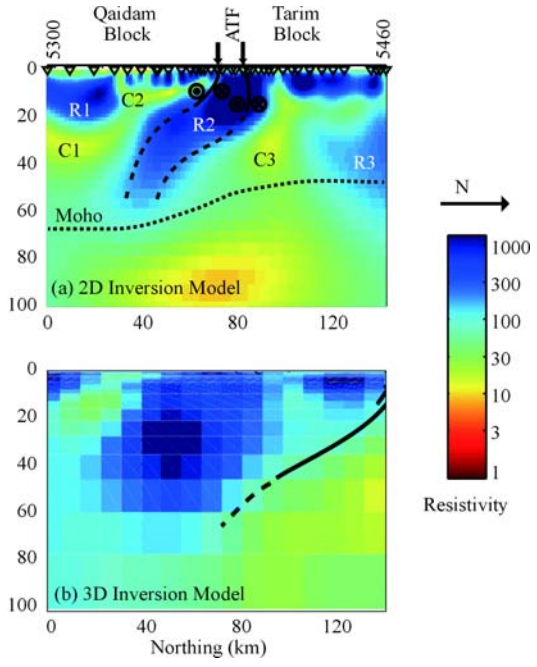

Fig. 8. Interpretation of the electrical structure model obtained from 2D inversion and its comparison with the 3D inversion model (the Moho depth is after Wang et al. (2005), Gao et al. (2009) and Xiao et al. (2011)).
Abbreviations are the same as in Fig.6.

model is mainly used for the qualitative study of the region with strong three-dimensionality in the southern section of the profile, as well as some off-profile electrical structures that cannot be resolved by 2D inversion. In the following section, we present a detailed analysis and discussion of the internal electrical structures of individual tectonic units.

6 Model Interpretations and Discussions

6.1 The Qaidam block

In the 2D inversion model of the northern section of the profile, the upper crust of the Qaidam block mainly exhibits a resistive feature (see R1 in Fig. 8a), and this resistive layer should represent the Precambrian crystalline basement of the Qaidam Basin. In the 3D inversion model,

a similar resistive layer is observed, although it is thinner than the feature obtained in the 2D inversion model (see Fig. 8b). This most likely occurs because the mesh of the 3D model is relatively coarse. The conductive layer overlying R1 should be the electrical representation of the shallow sediments of the Qaidam Basin, whereas the underlying conductive layer C1 likely characterizes the weak mid-lower crust beneath the Qaidam Basin on the northern margin of the Tibetan Plateau. Conductors C1 and C2 constitute a group of conductive layer with a south-dipping trend, most likely characterizing an intra-crust detachment surface within the Tibetan Plateau. The shallow conductor C2 might be caused by fluid inside the fracture zone formed on the northern margin of the plateau by the southward underthrust of the rigid Tarim block, whereas conductor C1 represents the weak mid-lower crust within the plateau. These two conductors are connected, forming the characteristic conductive layer of intra-crustal detachment surface within the plateau.

6.2 Altyn Tagh fault

In previous MT studies of the eastern section of ATF, the fault is mainly manifested by a sub-vertical interface of electrical properties (Bedrosian et al., 2001; Xiao et al., 2011). To the south of this interface, subsurface electrical structure beneath the ATF exhibits resistive, and the region to its north mainly exhibits conductive. The electrical structure model of this paper also reflects these features (see Fig. 8a). The two branches of the ATF mainly present as a sub-vertical electrical interface in the shallow upper crust but are gradually transformed to the south-dipping trend in the deep mid-lower crust, which forms the distribution pattern of resistor R2. Furthermore, it can be found that most electrical bodies from the profile exhibit the south-dipping trend (such as the aforementioned conductive layer constituted jointly by conductors C1 and C2); accordingly, it is inferred that these features might be related to the southward underthrust of the Tarim block. Meanwhile, there is no observation of lithospheric scale electrical anomalies from the 2D inversion model of the northern section of the profile, as shown in Fig. 8a, which indicates that the eastern section of the ATF only fractures on the intra-crust scale. Previous studies of the surface geology found that evidence of Quaternary basalt eruption in the eastern section of the ATF is lacking (Burchfiel et al., 1989). Therefore, this surface geological feature is very likely the result of the fact that the cutting depth in the eastern section of the ATF does not reach the mantle zone.

6.3 The Tarim block

According to the interpretation given by Xiao et al. (2011) with respect to the electrical structure model, the resistive mantle structure beneath the Tarim block indicates features of ancient and rigid lithosphere, supporting the tectonic model that the Tarim block underthrust beneath the ATF. Based on the 2D inversion model for the northern section of the profile, as generated in this study, this underthrusting structure is very unlikely on the lithospheric scale beneath the eastern section of the ATF. According to the contact between resistor R3 and conductor C3 in Fig. 8a, R3, which characterizes the crystalline basement of the rigid Tarim block, is only wedged into the mid-lower crust beneath the northern margin of the plateau, without experiencing subduction on the lithospheric scale. Conductor C3 characterizes the weak domain formed by this wedging process.

6.4 The North Qaidam thrust belt

The above interpretation of the subsurface structures is based on 2D inversion model. We did not perform 2D inversion for the southern section of the profile due to strong 3D effect, whereas 3D inversion used data from the overall profile. In this section, we qualitatively analyze the tectonic structures in the southern section of the profile based on 3D inversion model.

The research results of Xiao et al. (2011) noted that a large scale conductive region resides in the eastern section of the ATF, within the depth range of Moho in the North Qaidam and South Qilian area to the south of the ATF. Accordingly, the authors concluded that these conductive regions might connect with each other, forming an intra-crustal weak layer on the northern margin of the Tibetan Plateau. According to the 3D model for the profile in this study (see Figs. 7a and 7c), this highly conductive region matches the range of C5 well. Previous studies have found samples of mantle sourced ultra-high-pressure (UHP) metamorphic rocks (including eclogite and garnet peridotite) within the North Qaidam thrust belt and thus outlined the North Qaidam UHP metamorphic zone (Yang et al., 2002; Xu et al., 2006; Zhang et al., 2007; Chen et al., 2012). This likely implies that subduction on the lithospheric scale once occurred in this region, causing the upwelling and exhumation of these mantle materials. Yang et al. (2009) classified the North Qaidam-South Altyn HP-UHP metamorphic zone as an Eo-Tethys (Early Paleozoic) HP-UHP metamorphic zone, and the authors believed that the zone recorded a complete plate convergent event that marked by the subduction of oceanic crust and the following continental crust. The formation of conductor C5, as reflected from the 3D inversion model of this study, is likely associated with the tectonic effect of the subduction zone on the

northern margin of the Qaidam Basin and most likely also provides the deep fluid conditions for the formation of the UHP metamorphic zone.

Additionally, according to the 3D inversion model shown in Fig. 7a, the distribution patterns of the individual conductors in the research area indicates that they are not very well connected, suggesting that the tectonic deformation pattern in this region is very likely dominated by localized deformation and that the rheological properties of the lithosphere on the northern margin of the Tibetan Plateau vary not only vertically but also horizontally. Previous deep seismic reflection study at the eastern end of the sinistral strike slip Kunlun fault also indicate similar rheological characteristics (Wang et al., 2011). Therefore, such rheological property is very likely a common feature at the end region of large-scale strike-slip fault zones.

6.5 Discussion on the lateral variation of cutting depth of the Altyn Tagh fault

Previous studies of gravity (Jiang et al., 2004) and seismic tomography (Wittlinger et al., 1998) indicate that the fault zone is of lithospheric scale near the central section of the ATF at 89°E, whereas the eastern section of the fault zone, as presented in this paper, only exhibits as a fault on the intra-crust scale (as shown in Fig. 8a). This distinction reflects the fact that the cutting depth of the ATF gradually decreases from west to east. In the electrical structure model derived by Xiao et al. (2011), it was found that the scale of the positive flower structure formed by shearing action along the ATF also tends to decrease gradually eastward. From 94.3°E to 96°E, the cutting depth of the ATF decreases by approximately 15 km. In the easternmost end of the ATF, a new MT sounding profile running through the Northern Qilian fault indicates that the ATF near 98°E is reflected to be only a vague electrical interface within the range of the upper crust (Xiao et al., 2012). These features indicate that the sinistral strike-slip movement along the ATF is likely absorbed gradually by a series of thrust faults within the Qilian tectonic domain, forming the cutting depth of the ATF that gradually decreases eastward. The aforementioned inference is consistent with the tendency identified based on surface geology (Meyer et al., 1996) and GPS observations (Shen et al., 2001), namely, that the sinistral strike-slip rate along the ATF gradually decreases toward the east.

7 Conclusions

(1) In this study, we investigated the MT sounding profile across the eastern section of the ATF running through the northern margin of the Tibetan Plateau, obtaining high-quality impedance tensor data on the lithospheric scale by combining broadband and long-period data collection, after data processing with standard routines. We comprehensively analyzed the dimensionality and regional strike direction of the MT sounding data using multiple tools, such as phase tensor, GB decomposition of impedance tensor, and induction vector. The results of our analysis indicate that the two-dimensionality of the data for the northern section of the profile is sufficient for two-dimensional inversion. We also determined the regional strike direction to be approximately NE 60°; whereas the southern section of the profile exhibits strong three-dimensionality due to the influence of the North Qaidam thrust belt. Therefore, we implemented 2D inversion for the northern section of the profile and 3D inversion for the overall profile data. Based on the electrical structure model derived from 2D and 3D inversions, we acquired a new understanding of the electrical structure of the crust and upper mantle beneath the eastern section of the ATF on the northern margin of the Tibetan Plateau.

(2) The 2D inversion model indicated that the conductive layer with a south-dipping trend, constituted by conductors C1 and C2 within the Qaidam block, characterizes a intra-crust detachment surface within the Tibetan Plateau. The two branches of the Altyn fracture are mainly exhibited as a sub-vertical electrical interface in the shallow upper crust and are gradually transformed into resistor R2, which has a south-dipping trend in the deep mid-lower crust. Most electrical bodies from the profile exhibit a south-dipping trend, and this feature is likely associated with the southward underthrust of the Tarim block. Resistor R3, which characterizes the rigid crystalline basement of the Tarim block, is wedged into the mid-lower crust of the northern margin of the plateau, without subduction on the lithospheric scale. Instead, conductor C3 characterizes the weak region formed by this wedging process.

(3) Conductor C5 is located in the depth range of mid-lower crust within the Qilian block to the east of the North Qaidam thrust belt, as reflected from the 3D inversion model. Its formation is likely related to the subduction zone on the northern margin of the Qaidam Basin and most likely provides the deep fluid conditions for the formation of the UHP metamorphic zone. Additionally, the distribution patterns of individual conductors from the 3D inversion model indicate that they are not very well connected with each

other. This feature indicates that the pattern of tectonic deformation of the study region is dominated by localized deformation and that the rheological property of the lithosphere on the northern margin of the Tibetan Plateau varies not only in the vertical direction but also in the horizontal direction.

(4) The results of this study indicated that the eastern section of the ATF is only exhibited as a fracture on the intra-crust scale. In addition to the findings of previous studies that the central section of the ATF is a lithospheric-scale fault, this result reflects the trend that the cutting depth of the ATF gradually decreases from west to east. These characteristics suggest that, at the eastern section of the ATF, sinistral strike-slip movement occurring along the fault may be gradually absorbed by a series of thrust faults within the Qilian tectonic domain, thus forming a scaling trend in which strike-slip movement decreases gradually toward the east.

Acknowledgements

This work was supported by grants from the National Natural Science Foundation of China (General Program No. 40974058), National Science Fund for Distinguished Young Scholars (No. 40904025 and 41404060), and Fundamental Research Funds for the Central Universities (2652014016). We would like to thank the National Natural Science Foundation of China, United States National Science Foundation, Science Foundation of Ireland (award 08/RFP/GEO1693 to AGJ), and Natural Science and Engineering Research Council (Canada) for financial support. Thanks are due to Prof. Larry Brown for his leadership of INDEPTH project, as well as Zhuoma Danzhu and our field crew for their hard work during the field campaign. Zhang Letian would like to thank the China Scholarship Council for funding his visit to the University of Alberta for this collaborative research (File No. 2010640041). Part of 3-D inversions of this study made use of the infrastructure and resources of AICT (Academic Information and Communication Technologies) of the University of Alberta. Two anonymous reviewers have made comments on the original manuscript, their constructive suggestions are highly appreciated.

Manuscript received Feb. 11, 2014
accepted Sept. 24, 2014
edited by Liu Lian and Liu Xinzhu

References

Bedrosian, P.A., Unsworth, M.J., and Wang Fei, 2001. Structure of the Altyn Tagh fault and Daxue Shan from magnetotelluric surveys: Implications for faulting associated with the rise of the Tibetan Plateau. *Tectonics*, 20(4): 474–486.

Bendick R., Bilham R., Freymueller J., Larson K. and Yin Guanghua, 2000. Geodetic evidence for a low slip rate in the Altyn Tagh fault system. *Nature*, 404(6773): 69–72.

Berdichevsky, M.N., 1999. Marginal notes on magnetotellurics. *Surveys Geophys.*, 20(3): 341–375.

Burchfiel, B.C., 2013. Tibetan Plateau: Progress, But Many First Order Questions Remain. *Acta Geologica Sinica* (English Edition), 87(s1): 4–7.

Burchfiel, B.C., Deng Qidong, Peter, M., Leigh, R., Wang Yipeng, Zhang Peizhen and Zhang Weiqi, 1989. Intracrustal detachment within zones of continental deformation. *Geology*, 17(8): 748–752.

Cai Juntao and Chen Xiaobin, 2010. Refined techniques for data processing and two-dimensional inversion in magnetotelluric II: Which data polarization mode should be used in 2D inversion. *Chinese J. Geophys.*, 53(11): 2703–2714 (in Chinese with English abstract).

Caldwell, T.G., Bibby H.M., and Brown, C., 2004. The magnetotelluric phase tensor. *Geophys. J. Intl.*, 158(2): 457–469.

Chen Danling, Liu Liang, Sun Yong, Sun Weidong, Zhu Xiaohui, Liu Xiaoming and Guo Cailian, 2012. Felsic veins within UHP eclogite at xitieshan in North Qaidam, NW China: Partial melting during exhumation. *Lithos*, 136–139(0): 187–200.

Chen Wangping, Chen Chuyung and Nábelek J.L., 1999. Present-day deformation of the Qaidam basin with implications for intra-continental tectonics. *Tectonophysics*, 305(1–3): 165–181.

Chen Xuanhua, Yin An, Gehrels, G.E., Cowgill, E.S., Grove, M., Harrison, T.M., and Wang Xiao-Feng, 2003. Two phases of Mesozoic north-south extension in the eastern Altyn Tagh range, northern Tibetan Plateau. *Tectonics*, 22(5): 1053.

Cowgill, E., Gold, R.D., Chen Xuanhua, Wang Xiaofeng, Arrowsmith, J R., and Southon, J., 2009. Low Quaternary slip rate reconciles geodetic and geologic rates along the Altyn Tagh fault, northwestern Tibet. *Geology*, 37(7): 647–650.

Cowgill E., Yin An, Harrison, T.M., and Wang Xiaofeng, 2003. Reconstruction of the Altyn Tagh fault based on U-Pb geochronology: Role of back thrusts, mantle sutures, and heterogeneous crustal strength in forming the Tibetan Plateau. *J. Geophys. Res.*, 108(B7): 2346.

Egbert G.D., 1997. Robust multiple-station magnetotelluric data processing. *Geophys. J. Intl.*, 130(2): 475–496.

Elliott, J.R., Biggs, J., Parsons, B., and Wright, T.J., 2008. InSAR slip rate determination on the Altyn Tagh Fault, northern Tibet, in the presence of topographically correlated atmospheric delays. *Geophys. Res. Lett.*, 35(12): L12309.

Gamble, T.D., Goubau, W.M., and Clarke, J., 1979. Magnetotellurics with a remote magnetic reference. *Geophysics*, 44(1): 53–68.

Gao Rui, Xiong Xiaosong, Li Qiusheng and Lu Zhanwu, 2009. The Moho depth of Qinghai-Tibet Plateau revealed by seismic detection. *Acta Geosci. Sinica*, 30(6): 761–773 (in Chinese with English abstract).

Gold, R.D, Cowgill, E., Arrowsmith, J.R., Chen Xuanhua, Sharp, W.D, Cooper, K.M., and Wang Xiaofeng, 2011. Faulted terrace risers place new constraints on the late Quaternary slip

rate for the central Altyn Tagh fault, northwest Tibet. *Geol. Soc. Am. Bull.*, 123(5–6): 958–978.

Groom, R.W., and Bailey, R.C., 1989. Decomposition of Magnetotelluric Impedance Tensors in the Presence of Local 3-Dimensional Galvanic Distortion. *J. Geophys Res.-Solid Earth Planets*, 94(B2): 1913–1925.

Jiang Xiaodian, Jin Yu and McNutt Marcia, K., 2004. Lithospheric deformation beneath the Altyn Tagh and West Kunlun faults from recent gravity surveys. *J. Geophys. Res.*, 109(B5): B05406.

Jin Sheng, Wei Wenbo, Ye Gaofeng, Deng Ming, Tan Handong and Unsworth Martyn, 2009. The electrical structure of Bangong-Nujiang suture: results from magnetotelluric sounding detection. *Chinese J. Geophys.*, 52(10): 2666–2675 (in Chinese with English abstract).

Jin Sheng, Ye Gaofeng, Wei Wenbo, Deng Ming and Jing Jianen, 2007. The Electrical Structure and Fault Feature of Crust and Mantle of Western Tibet Plateau: Based on Results of Magnetotelluric Survey along Profile Zhada-Quanshuihu. *Earth Sci. —J. China Univ. Geosci.*, 32(4): 474–480 (in Chinese with English abstract).

Jin Sheng, Ye Gaofeng, Wei Wenbo, Deng Ming and Unsworth Martyn, 2006. The electrical structure and fault feature of crust of south-eastern Tibetan Plateau—the results of magnetotelluric prospecting on profile from Xiachayu-Changdu. *Earth Sci. Frontiers*, 13(5): 408–415 (in Chinese with English abstract).

Karplus, M.S., Klemperer, S.L., Lawrence, J.F., Zhao, W., Mechie, J., Tilmann, F., Sandvol, E. and Ni, J., 2013. Ambient-noise tomography of north Tibet limits geological terrane signature to upper-middle crust. *Geophys. Res. Lett.*, 40(5): 808–813.

Karplus, M.S., Zhao, W., Klemperer, S.L., Wu, Z., Mechie, J., Shi, D., Brown, L.D. and Chen, C., 2011. Injection of Tibetan crust beneath the south Qaidam Basin: Evidence from INDEPTH IV wide-angle seismic data. *J. Geophys. Res.*, 116 (B7): B07301.

Le Pape, F., Jones, A.G., Vozar, J., and Wenbo Wei, 2012. Penetration of crustal melt beyond the Kunlun Fault into northern Tibet. *Nature Geosci*, 5(5): 330–335.

Ledo Juanjo, 2005. 2-D Versus 3-D Magnetotelluric Data Interpretation. *Surveys Geophys.*, 26(5): 511–543.

McNeice, G.W., and Jones, A.G., 2001. Multisite, multifrequency tensor decomposition of magnetotelluric data. *Geophysics*, 66(1): 158–173.

Mechie, J., Zhao, W., Karplus, M.S., Wu, Z., Meissner, R., Shi, D., Klemperer, S.L., Su, H., Kind, R., Xue, G., and Brown, L.D., 2012. Crustal shear (S) velocity and Poisson's ratio structure along the INDEPTH IV profile in northeast Tibet as derived from wide-angle seismic data. *Geophys. J. Intl.*, 191 (2): 369–384.

Mériaux, A.S., Ryerson, F.J., Tapponnier, P., Van der Woerd, J., Finkel, R.C., Xu Xiwei, Xu Zhiqin and Caffee, M.W., 2004. Rapid slip along the central Altyn Tagh Fault: Morphochronologic evidence from Cherchen He and Sulamu Tagh. *J. Geophys. Res.: Solid Earth*, 109(B6): B06401.

Mériaux, A.S., Tapponnier, P., Ryerson, F.J., Xiwei Xu, King, G., Van der Woerd, J., Finkel, R.C., Haibing, Li, Caffee, M.W., Zhiqin Xu and Wenbin Chen, 2005. The Aksay segment of the northern Altyn Tagh fault: Tectonic geomorphology, landscape evolution, and Holocene slip rate. *J. Geophys. Res.: Solid Earth*, 110(B4): B04404.

Meyer, B., Tapponnier, P., Gaudemer, Y., Peltzer, G., Guo Shunmin and Chen Zhitai, 1996. Rate of left-lateral movement along the easternmost segment of the Altyn Tagh fault, east of 96°E (China). *Geophys. J. Intl.*, 124(1): 29–44.

Miensopust, M.P., Queralt, P., Jones, A.G., and 3D MT modellers, 2013. Magnetotelluric 3-D inversion—a review of two successful workshops on forward and inversion code testing and comparison. *Geophys. J. Intl.*, 193(3): 1216–1238.

Moorkamp, M., 2007. Comment on 'The magnetotelluric phase tensor' by T. Grant Caldwell, Hugh M. Bibby and Colin Brown. *Geophys. J. Intl.*, 171(2): 565–566.

Nelson, K.D., Zhao Wenjin, Brown, L.D., Kuo, J., Che Jinkai, Liu Xianwen, Klemperer, S.L., Makovsky, Y., Meissner, R., Mechie, J., Kind, R., Wenzel, F., Ni, J., Nabelek, J., Chen Leshou, Tan Handong, Wei Wenbo, Jones, A.G., Booker, J., Unsworth, M., Kidd, W.S. F., Hauck, M., Alsdorf, D., Ross, A., Cogan, M., Wu Changde, Sandvol, E., and Edwards, M., 1996. Partially Molten Middle Crust Beneath Southern Tibet: Synthesis of Project INDEPTH Results. *Science*, 274(5293): 1684–1688.

Parkinson, W., 1959. Directions of Rapid Geomagnetic Fluctuations. *Geophys. J. R. Astr. Soc.*, 2(1): 1–14.

Peltzer, G., and Tapponnier, P., 1988. Formation and Evolution of Strike-Slip Faults, Rifts, and Basins During the India-Asia Collision: An Experimental Approach. *J. Geophys. Res.*, 93 (B12): 15085–15117.

Peltzer, G., Tapponnier, P., and Armijo, R., 1989. Magnitude of Late Quaternary Left-Lateral Displacements Along the North Edge of Tibet. *Science*, 246(4935): 1285–1289.

Ritts B.D., and Biffi, U., 2000. Magnitude of post–Middle Jurassic (Bajocian) displacement on the central Altyn Tagh fault system, northwest China. *Geol.Soc.Am. Bull.*, 112(1): 61–74.

Rodi, W., and Mackie, R.L., 2001. Nonlinear conjugate gradients algorithm for 2-D magnetotelluric inversion. *Geophysics*, 66 (1): 174–187.

Shen Zhengkang, Wang Min, Li Yanxing, Jackson, D.D., Yin An, Dong Danan and Fang Peng, 2001. Crustal deformation along the Altyn Tagh fault system, western China, from GPS. *J. Geophys. Res.*, 106(B12): 30607–30621.

Siripunvaraporn, W., 2011. Three-Dimensional Magnetotelluric Inversion: An Introductory Guide for Developers and Users. *Surveys Geophys.* 1–23.

Siripunvaraporn, W., Egbert, G., Lenbury, Y., and Uyeshima, M., 2005a. Three-dimensional magnetotelluric inversion: data-space method. *Physics Earth Planet. Interiors*, 150(1–3): 3–14.

Siripunvaraporn, W., Egbert, G. and Uyeshima, M., 2005b. Interpretation of two-dimensional magnetotelluric profile data with three-dimensional inversion synthetic examples. *Geophys. J. Intl.*, 160(3): 804–814.

Styron, R., Taylor, M., and Okoronkwo, K., 2010. Database of Active Structures From the Indo-Asian Collision. *Eos Trans. AGU*, 91(20): 181–182.

Tan Handong, Wei Wenbo, Unsworth, M., Deng Ming, Jin Sheng, Booker, J., and Jones, A., 2004. Crustal electrical conductivity structure beneath the Yarlung Zangbo Jiang suture in the southern Xizang plateau. *Chinese J. Geophys.*, 47 (4): 685–690 (in Chinese with English abstract).

Tilmann, F., Ni, J., and INDEPTH III Seismic Team, 2003.

Seismic Imaging of the Downwelling Indian Lithosphere Beneath Central Tibet. *Science*, 300(5624): 1424–1427.

Unsworth, M., Jones, A.G., Wei, W., Marquis, G., Gokarn, S.G. and Spratt, J. E., 2005. Crustal rheology of the Himalaya and Southern Tibet inferred from magnetotelluric data. *Nature*, 438(7064): 78–81.

Wallace, K., Yin Guanghua and Bilham, R., 2004. Inescapable slow slip on the Altyn Tagh fault. *Geophys. Res. Lett.*, 31(9): L09613.

Wang Chengshan, Gao Rui, Yin An, Wang Haiyan, Zhang Yuxiu, Guo Tonglou, Li Qusheng and Li Yalin, 2011. A mid-crustal strain-transfer model for continental deformation: A new perspective from high-resolution deep seismic-reflection profiling across NE Tibet. *Earth Planet. Sci. Lett.*, 306(3–4): 279–288.

Wang Youxue, Mooney, W.D., Han Guohua, Yuan Xuecheng and Jiang Mei, 2005. The Crustal P-Wave Velocity Structure From Altyn Tagh to Longmen Mountains along the Taiwan-Altay Geoscience Transect. *Chinese J. Geophys*., 48(1): 98–106 (in Chinese with English abstract).

Washburn, Z., Arrowsmith, J.R., Dupont-Nivet, G., Feng, W.X., Qiao, Z.Y. and Chen Z., 2003. Paleoseismology of the Xorxol Segment of the Central Altyn Tagh Fault, Xinjiang, China. *Annals of Geophysics*, 46(5): 1015–1034.

Wei Wenbo, Jin Sheng, Ye Gaofeng, Deng Ming, Jing Jianen, Unsworth, M., and Jones, A., 2009. Conductivity structure and rheological property of lithosphere in Southern Tibet inferred from super-broadband magnetotelluric sounding. *Sci. China* (D)-*Earth Sci.*, 39(11): 1591–1606 (in Chinese with English abstract).

Wei Wenbo, Jin Sheng, Ye Gaofeng, Deng Ming, Tan Handong, Unsworth, M., Booker, J., and Jones, A., 2006a. Features of the Faults in Center and North Tibetan Plateau: Based on Results of INDEPTH (III)-MT. *Earth Science —J. China Univ. Geosci.*, 31(2): 257–265 (in Chinese with English abstract).

Wei Wenbo, Jin Sheng, Ye Gaofeng, Deng Ming, Tan Handong, Unsworth, M., Jones, A. and Booker, J., 2006b. Conductivity structure of crust and upper mantle beneath the northern Tibetan Plateau: Results of super-wide band magnetotelluric sounding. *Chinese J. Geophys.*, 49(4): 1215–1225 (in Chinese with English abstract).

Wei Wenbo, Unsworth, M., Jones, A., Booker, J., Tan Handong, Nelson, D., Chen Leshou, Li Shenghui, Solon, K., Bedrosian, P., Jin Sheng, Deng Ming, Ledo, J., Kay, D., and Roberts, B., 2001. Detection of Widespread Fluids in the Tibetan Crust by Magnetotelluric Studies. *Science*, 292(5517): 716–719.

Wittlinger, G., Tapponnier, P., Poupinet, G., Mei Jiang, Danian Shi, Herquel, G. and Masson, F., 1998. Tomographic Evidence for Localized Lithospheric Shear Along the Altyn Tagh Fault. *Science*, 282(5386): 74–76.

Xiao Qibin, Zhang Jin, Wang Jijun, Zhao Guoze and Tang Ji, 2012. Electrical resistivity structures between the Northern Qilian Mountains and Beishan Block, NW China, and tectonic implications. *Physics Earth Planet Interiors*, 200–201(0): 92–104.

Xiao Qibin, Zhao Guoze and Dong Zeyi, 2011. Electrical resistivity structure at the northern margin of the Tibetan Plateau and tectonic implications. *J. Geophys. Res.*, 116(B12): B1, 2401.

Xu Zhiqin, Burg, J.P., Wang Qin and Li Haibing, 2013. Indo-Asian Collision: Transition from Compression to Lateral Escape Tectonics. *Acta Geologica Sinica* (English Edition), 87(s1): 112–113.

Xu Zhiqin, Yang Jingsui, Wu Cailai, Li Haibing, Zhang Jianxin, Qi Xuexiang, Song Shuguang and Qiu Haijun, 2006. Timing and mechanism of formation and exhumation of the Northern Qaidam ultrahigh-pressure metamorphic belt. *J. Asian Earth Sci.*, 28(2–3): 160–173.

Yang Jingsui, Xu Zhiqin, Zhang Jianxin, Song Shuguang, Wu Cailai, Shi Rendeng, Li Haibing and Brunel, M., 2002. Early Palaeozoic North Qaidam UHP metamorphic belt on the north-eastern Tibetan plateau and a paired subduction model. *Terra Nova*, 14(5): 397–404.

Yang Jingsui, Xu Zhiqin, Zhang Jianxin, Zhang Zeming, Liu Fulai and Wu Cailai, 2009. Tectonic setting of main high-and ultrahigh-pressure metamorphic belts in China and adjacent region and discussion on their subduction and exhumation mechanism. *Acta Petrol. Sinica*, 25(7): 1529–1560 (in Chinese with English abstract).

Ye Gaofeng, Jin Sheng, Wei Wenbo and Unsworth, M., 2007. Research of Conductive Structure of Crust and Upper Mantle beneath the South-Central Tibetan Plateau. *Earth Science —J. China Univ. Geosci.*, 32(4): 491–498 (in Chinese with English abstract).

Zhang Jianxin, Meng Fancong and Mattinson, C.G., 2007. Progress, Controversies and Challenge of Studies on South Altyn Tagh-North Qaidam HP/UHP Metamorphic Belt. *Geol. J. China Univ.*, 13(3): 526–545 (in Chinese with English abstract).

Zhang Peizhen, Molnar, P. and Xu Xiwei, 2007. Late Quaternary and present-day rates of slip along the Altyn Tagh Fault, northern margin of the Tibetan Plateau. *Tectonics*, 26(5): TC5010.

Zhang Peizhen, Shen Zhengkang, Wang Min and Gan Weijun, 2004. Kinematics of Present-Day Tectonic Deformation of the Tibetan Plateau and Its Vicinities. *Seismol. Geol.*, 26(3): 367–377 (in Chinese with English abstract).

About the first author

ZHANG Letian Male; born in 1982; Post-doctoral Research Fellow at China University of Geosciences (Beijing). He is now doing research on tectonophysics of the Tibetan Plateau mainly by using the magnetotelluric method.

E-mail: letianOI@163.com.